Transmission to reflection transformation of teleseismic wavefields

M. Ravi Kumar[1] and M. G. Bostock[2]

Received 11 October 2005; revised 5 April 2006; accepted 5 May 2006; published 17 August 2006.

[1] In this paper we review the transformation of *P* and *SV* transmission Green's functions into the corresponding reflection quantities for one-dimensional, elastic media at precritical slownesses. To obtain estimates of the transmission Green's functions from observed data, we apply a recently developed approach that exploits the minimum-phase nature of the direct waves and employs autospectra and cross-spectra of raw component seismograms representing multiple sources recorded at a single station. To accomplish transformation to reflection Green's functions, we outline a practical recipe that involves amplitude balancing, energy normalization, cross correlation, and removal of free surface effects. We assess its performance through application to both synthetic seismograms and data from station Hyderabad. In all cases we are able to identify the first-order scattering contributions from the continental Moho. The transmission-to-reflection transformation has potential applications for imaging hitherto elusive shallow mantle discontinuities, since interfering forward and back scattering contributions are effectively separated by component in the resulting reflection Green's functions.

Citation: Kumar, M. R., and M. G. Bostock (2006), Transmission to reflection transformation of teleseismic wavefields, *J. Geophys. Res.*, *111*, B08306, doi:10.1029/2005JB004104.

1. Introduction

[2] Over the past few decades, studies employing teleseismic *P*-to-*S* (*Ps*) converted waves, have provided invaluable information on subsurface structure. Application of the receiver function approach to earthquake recordings from both single station and array deployments have enabled mapping of the crustal (Moho) and the upper mantle (410 and 660 km) discontinuities in unprecedented detail, narrowing the gap between high-frequency active seismic and low-frequency surface wave studies. However, since the pioneering work of *Vinnik* [1977], dealing with detection of the *P*-to-*SV* converted waves from the mantle discontinuities, the problem of interference between forward scattered (e.g., converted) and back-scattered (multiples) waves has severely hampered resolution of structure in the upper most mantle. This shortcoming arises because the timing of *Ps* conversions from discontinuities in the depth range of 100–250 km (e.g., Lehmann, lithospheric asthenospheric boundary), coincides with that of multiples from shallower crustal interfaces, particularly the Moho, thereby masking their detection. Although some efforts have been made to overcome this problem through the use of *S*-to-*P* converted waves [e.g., *Farra and Vinnik*, 2000; *Vinnik et al.*, 2005; *Kumar et al.*, 2005] where direct conversions and free surface multiples are separated on either side of the incident *S* wave, the small number and low signal-to-noise ratios of suitable *S* wave recordings frequently limit their utility.

[3] A conceptually attractive means of isolating the different scattering contributions involves transforming the transmission response of a medium into its reflection response, as originally proposed by *Claerbout* [1968]. For a horizontally layered medium, he demonstrated that one side of the autocorrelation of an acoustic seismogram recorded by a surface receiver due to a plane wave source at depth is the reflection response due to a surface plane wave source recorded by the same receiver. Extensions of this approach to one-dimensional elastic [*Frasier*, 1970] and fully three-dimensional elastic [*Wapenaar et al.*, 2004] media have been subsequently derived. In the case of laterally heterogeneous media, the procedure requires cross correlations of recordings of the surface wavefield at two different locations arising from multiple sources in the subsurface. Recently there has been considerable interest in the related topic of Green's function extraction from ambient noise, in particular, as applied to surface wave tomography [e.g., *Campillo and Paul*, 2003; *Sabra et al.*, 2005; *Shapiro et al.*, 2005]. However, with the exception of a local, short-period study in Hawaii employing vertical component recordings [*Daneshvar et al.*, 1995], applications of transmission-to-reflection transformation have, to date, been limited to numerical simulations.

[4] In this study we review the theoretical formulation for synthesis of the one-dimensional (1-D) reflection response of a horizontally stratified medium and provide a recipe for practical synthesis using teleseismic *P* and *SV* Green's functions. We demonstrate its application using both nu-

[1]National Geophysical Research Institute, Hyderabad, India.
[2]Department of Earth and Ocean Sciences, The University of British Columbia, Vancouver, British Columbia, Canada.

0148-0227/06/2005JB004104$09.00

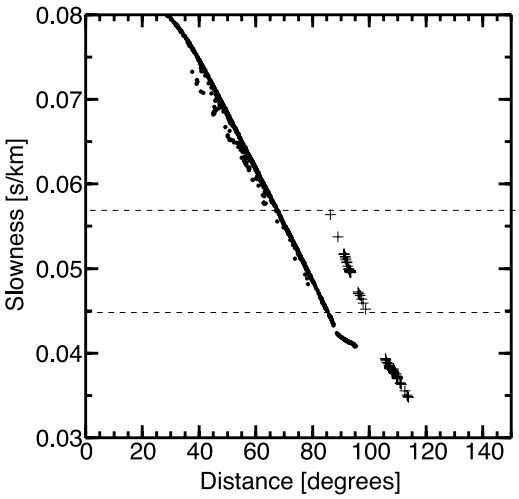

Figure 1. Slowness values of *P* (dots) and *SKS* (pluses) phases with respect to epicentral distance for good quality waveforms recorded at Hyderabad. Dashed lines indicate the overlapping slowness range.

merical simulations and data from GEOSCOPE station at Hyderabad.

2. Data

[5] Since our emphasis is on synthesis of the 1-D reflection response from teleseismic (transmission) recordings, we shall require that the recording station is underlain by a predominantly 1-D structure that has remained in operation for sufficient time to produce large numbers of *P* and *SV* waveform data. The GEOSCOPE station at Hyderabad (HYB) fulfills these conditions making it ideal for this analysis. The station has been in operation since 1989 and is sited on Precambrian granites that form a large portion of the central Indian shield. It is equipped with a very broadband STS1 sensor and produces data of high quality. The crust beneath HYB is known to be simple with a large velocity contrast across the Moho [*Saul et al.*, 2000]. Another basic requirement for the analysis is that *P* and *S* responses are available at comparable slowness (or ray parameter) and frequency. Waveforms of teleseismic *P* from events in the distance range 65–98° are characterized by slowness comparable to that of *SKS* in the range 84–100° making their combination appropriate for our purposes (Figure 1). In general, however, the bandwidth available for teleseismic *S* is considerably reduced at high frequencies (>0.2 Hz) relative to *P*, owing to higher attenuation in the upper mantle, and it is necessary to restrict attention to seismograms from deep events to minimize this inconsistency. Thus, whereas it is relatively easy to obtain large numbers of high-quality *P* waveforms from most permanent stations, *SKS* waveforms of comparable quality are decidedly more difficult to come by.

3. Green's Functions

[6] We recover the Green's function response due to a teleseismic *P* wave, by applying the method of *Baig et al.* [2005], an extension of that originally proposed by *Bostock* [2004], to exploit multiple source-receiver configurations. In this approach, the minimum phase character of the *P* phase is employed to remove the source effect from the seismograms using the autospectra and cross-spectra of seismograms from multiple sources recorded at the same station (HYB in the present study). As an a priori requirement for the removal of source effects, the (upgoing) *P*, *SV* and *SH* components of the wavefield are obtained from the raw horizontal and vertical displacement components by applying the 1-D wavefield decomposition scheme of *Kennett* [1991]. The high quality of data and the extended duration of operation have resulted in suitable *P* waveforms from nearly 1200 teleseismic events for this analysis. We have divided these three component waveforms into 100 horizontal slowness bins (average of 12 seismograms per bin) between 0.04 and 0.08 s/km. The source signatures represented by seismograms in individual bins are then simultaneously deconvolved to obtain Green's functions at the corresponding slowness values. The high-quality *P* and *SV* components of the recovered teleseismic *P* Green's functions are evident from Figures 2a and 2b and clearly reveal the major scattered phases from the continental Moho, specifically, Pp_Mp (~10 s in Figure 2a) and P_Ms, Pp_Ms and Ps_Ms (~4 s, ~13 s and ~17 s, respectively in Figure 2b). Each of these phases can be traced across the entire slowness range.

[7] The procedure for obtaining the Green's function response due to a teleseismic *S* wave, is conceptually similar to that used for estimating the *P* Green's functions. In this

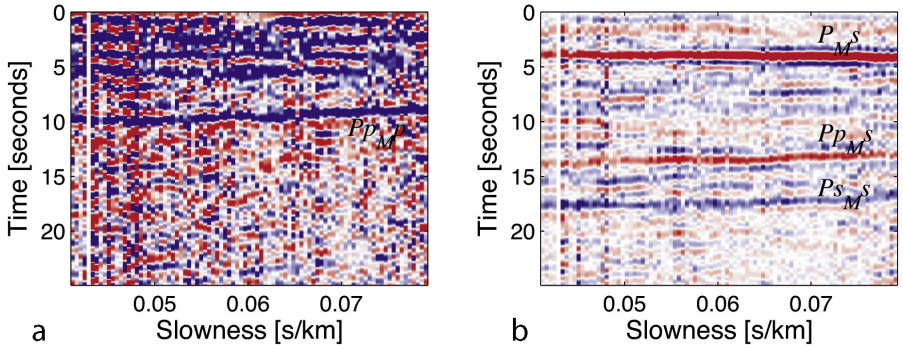

Figure 2. Image of the (a) *P* and (b) *SV* components of the teleseismic *P* Green's functions, as a function of slowness, for station Hyderabad. The forward (P_Ms) and the backscattered (Pp_Mp, Pp_Ms, Ps_Ms) phases are strong and can be traced across the whole slowness range.

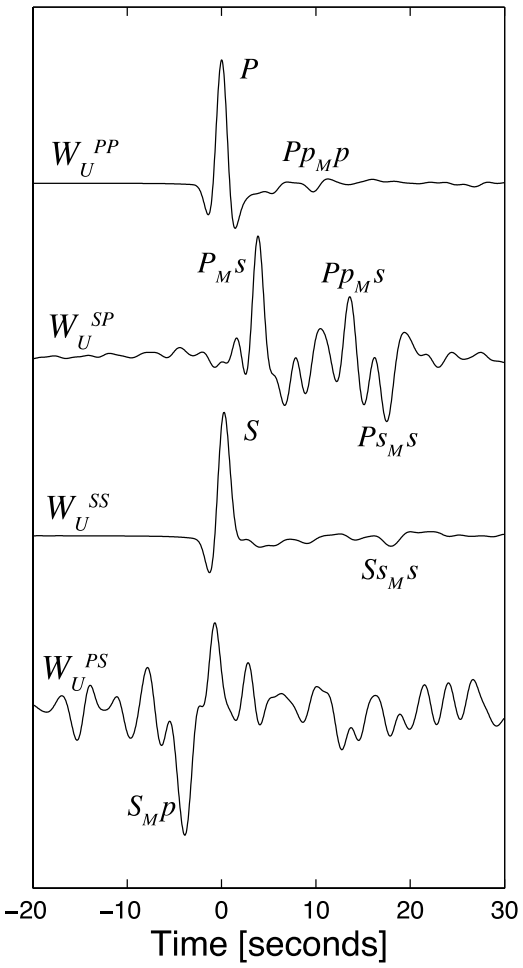

Figure 3. Single estimates of *P* and *SV* component Green's functions for station HYB in a comparable slowness range of 0.04–0.057 s/km, used for synthesis of equivalent reflection seismograms. The waveforms are band-pass filtered in the range of 0.02–0.5Hz. The Green functions reveal most of the forward and backscattered phases.

case, the source response is recovered by exploiting the minimum phase character of the main incident *S* phase [*Bostock*, 2006]. As discussed by *Bostock* [2004], the minimum phase property of teleseismic *S* is, in principle, more approximate than for *P* due to the presence of doubly scattered *S-P-S* precursory arrivals. In practice, however, such precursory phases involve two consecutive scattering interactions, leading to amplitudes generally below other signal-generated noise levels, and so, may be ignored in a single scattering context. For isotropic media, as assumed here, wherein *P-SV* propagation is decoupled from that of *SH*, estimation of the Green's function proceeds in a manner analogous to that for teleseismic *P* with the roles of *P* and *SV* interchanged (*Bostock* [2006] discusses additional factors to be considered for anisotropic media; see also *Farra and Vinnik* [2000]). A set of linear equations is constructed using auto and cross-correlation spectra of various combinations of three-component *S* waveforms from different sources recorded at the same station. Estimates for the power spectra of the source time functions are obtained by spectral smoothing and incorporated within these equations. Solution of the linear system yields the spectra of the *P*, *SV* and *SH* components of the teleseismic *SV* Green's functions (and sources). The minimum phase condition is applied to *SV* whereas the phase of the original seismograms is used to recreate the phase of the remaining *P* and *SH* Green's function components in the final step (see *Mercier et al.* [2006] for details).

[8] The number (30) of *SKS* recordings suitable for our purposes is far smaller than that (300) for teleseismic *P*. We therefore content ourselves with producing a single estimate of the corresponding *SV* Green's function at a nominal slowness of 0.047 s/km using recordings over the slowness range (0.04–0.057 s/km). The individual Green's function estimates for both *P* and *SV* incidence are shown in Figure 3 and will be used in section 5.2 to synthesize equivalent reflection seismograms. Before doing so, however, we shall review the underlying theory.

4. Synthesizing the Reflection Response

4.1. Concept

[9] We begin this section with a brief summary of transmission-to-reflection transformation in the 1-D, elastic context as previously described by *Frasier* [1970]. Let us first consider the plane wave, frequency domain response of a stratified half-space to incident plane *P* and *SV* wavefields (at a given frequency ω and slowness p) excited at the free surface and that we shall identify through the respective columns of the identity matrix I (see Figure 4). The symbols V_U and V_D are used to denote the upgoing and downgoing wave vector matrices that describe the resulting wavefield

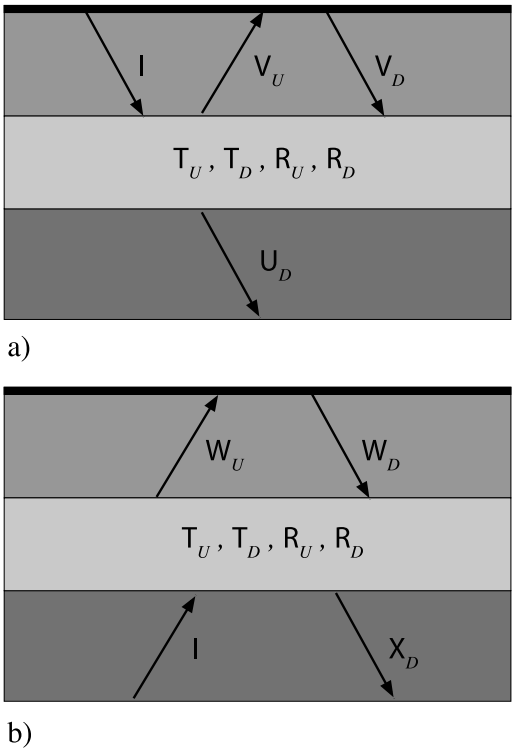

Figure 4. Representation of quantities used for transformation of plane wave transmission wavefield into a plane wave reflection wavefield.

above the stratification whereas U_D is the corresponding quantity representing the downgoing wavefield in the homogeneous half-space below the stratification. These quantities can be expressed in terms of the reflection/transmission matrices [*Kennett*, 1983] for stratification without the free surface as

$$\mathsf{V}_U = \left[\mathsf{I} - \mathsf{R}_D\tilde{\mathsf{R}}\right]^{-1}\mathsf{R}_D, \tag{1}$$

$$\mathsf{V}_D = \mathsf{I} + \tilde{\mathsf{R}}\left[\mathsf{I} - \mathsf{R}_D\tilde{\mathsf{R}}\right]^{-1}\mathsf{R}_D = \mathsf{I} + \tilde{\mathsf{R}}\mathsf{V}_U, \tag{2}$$

and

$$\mathsf{U}_D = \mathsf{T}_D\left[\mathsf{I} + \tilde{\mathsf{R}}\left[\mathsf{I} - \mathsf{R}_D\tilde{\mathsf{R}}\right]^{-1}\mathsf{R}_D\right] = \mathsf{T}_D\mathsf{V}_D. \tag{3}$$

The quantity R_D is the reflection matrix for downward incidence upon the stratification, T_U is the transmission matrix for upward incidence upon the stratification, and $\tilde{\mathsf{R}}$ is the free surface reflection matrix. The quantity $\left[\mathsf{I} - \mathsf{R}_D\tilde{\mathsf{R}}\right]^{-1}$ is the reverberation operator that accounts for the infinite sequence of multiple reflections generated between the free surface and the underlying structure.

[10] Conservation of vertical energy flux for waves at precritical slowness traversing the stratification allows us to set the flux immediately below the surface and that below the stratification to be equal; accordingly, we may write

$$\mathsf{V}_D^\dagger\mathsf{V}_D - \mathsf{V}_U^\dagger\mathsf{V}_U = \mathsf{I} + \tilde{\mathsf{R}}\mathsf{V}_U + \mathsf{V}_U^\dagger\tilde{\mathsf{R}}^\dagger = \mathsf{U}_D^\dagger\mathsf{U}_D, \tag{4}$$

where the dagger denotes complex conjugate transpose, and we have assumed that all quantities are referred to wave vector bases that have been normalized with respect to vertical energy flux [e.g., *Kennett*, 1983].

[11] We now consider the reciprocal experiment for which an impulsive wavefield is incident upon the same free surface bounded stratification from below (Figure 4b). We represent the resulting wavefield recorded at the surface by a vector matrix W_U comprising the two upgoing column wave vectors that represent the impulse response to incident *P* wave and *S* wave sources. By reciprocity, we have $\mathsf{W}_U = \mathsf{U}_D^{\mathrm{T}}$ such that

$$\mathsf{W}_U^*\mathsf{W}_U^{\mathrm{T}} = \mathsf{I} + \tilde{\mathsf{R}}\mathsf{V}_U + \mathsf{V}_U^\dagger\tilde{\mathsf{R}}^\dagger, \tag{5}$$

where the asterisk denotes complex conjugate and superscript T indicates transposition. The quadratic form on the left-hand side of (5) comprises complex conjugated quantities thereby implying sums of autocorrelations and cross correlations of seismograms in the time domain. The first term on the right-hand side of (5) corresponds to an impulse (on the diagonal components) at zero time in the time domain, whereas the second and third terms are purely causal and acausal contributions, respectively. Hence we recognize that by measuring the appropriate responses (i.e., due to both *P* and *S* sources at constant *p*) for the earthquake geometry (i.e., plane wave from below), one may recover, through cross correlation and a simple windowing operation, the result of a corresponding reflection experiment, namely, V_U, for which the source wavefield is incident from above. Note that for normal incidence in isotropic media *P* and *SV* interactions are decoupled and so only autocorrelations of single component wavefields are required.

4.2. Practical Recipe

[12] Although the formulation in section 4.1 applies to generally anisotropic, 1-D elastic media, our analysis will be restricted to a 1-D isotropic medium. Accordingly, the upgoing wavefield matrix W_U is represented by a 2×2 matrix wherein the individual elements are ordered as

$$\mathsf{W}_U = \begin{bmatrix} W_U^{PP} & W_U^{PS} \\ W_U^{SP} & W_U^{SS} \end{bmatrix}, \tag{6}$$

such that the first column represents the wave components of the Green's function due to an incident teleseismic *P* wave and the second column contains the components due to an incident *SV* (*SKS*) wave. A practical recipe for combining these components to synthesize the reflection response comprises four essential steps, namely, (1) amplitude balancing, (2) energy normalization, (3) cross correlation, and (4) removal of the free surface effect, as we describe below:

4.2.1. Amplitude Balancing

[13] We shall assume that the incident upgoing wavefields due to individual *P* and *S* sources are similarly affected by the medium heterogeneity such that the amplitudes of the direct *P* and *S* waves at the surface are equivalent for corresponding incident waves of equal magnitude. This assumption is necessary because the true amplitudes of incident *P* and *SV* waves at the base of the stratification are not known and the amplitudes of the two columns of W_U must be proportionally balanced.

[14] Accordingly, we set

$$\begin{aligned} W_U^{SP} &\Leftarrow \frac{W_U^{PP}}{\max\left(W_U^{PP}\right)} \qquad W_U^{SP} \Leftarrow \frac{W_U^{PP}}{\max\left(W_U^{PP}\right)}, \\ W_U^{SS} &\Leftarrow \frac{W_U^{SS}}{\max\left(W_U^{SS}\right)} \qquad W_U^{PS} \Leftarrow \frac{W_U^{PS}}{\max\left(W_U^{SS}\right)}, \end{aligned} \tag{7}$$

where left arrow denotes redefinition and is used to avoid notational complexity that would result from introduction of new symbols.

4.2.2. Energy Normalization

[15] Equation (5) was derived for loss-less media under the assumption that the wavefields have been normalized by vertical energy flux. Our next step is thus to define the normalization factors

$$\begin{aligned} C_m^\alpha &= \sqrt{\rho_m\alpha_m^2 q_m^\alpha} \qquad C_s^\alpha = \sqrt{\rho_s\alpha_s^2 q_s^\alpha}, \\ C_m^\beta &= \sqrt{\rho_m\beta_m^2 q_m^\beta} \qquad C_s^\beta = \sqrt{\rho_s\beta_s^2 q_s^\beta}, \end{aligned} \tag{8}$$

where subscripts *s* and *m* identify the properties immediately below the free surface and stratification, respectively. Similarly, α, β, ρ denote material properties *P* velocity, *S* velocity, and density, respectively, and the vertical slowness of *P* and *S* waves at, e.g., the Earth's surface, are given by q_s^α, q_s^β. Note that the normalization factors below the stratification (i.e., C_m^α, C_m^β) must once more be assumed,

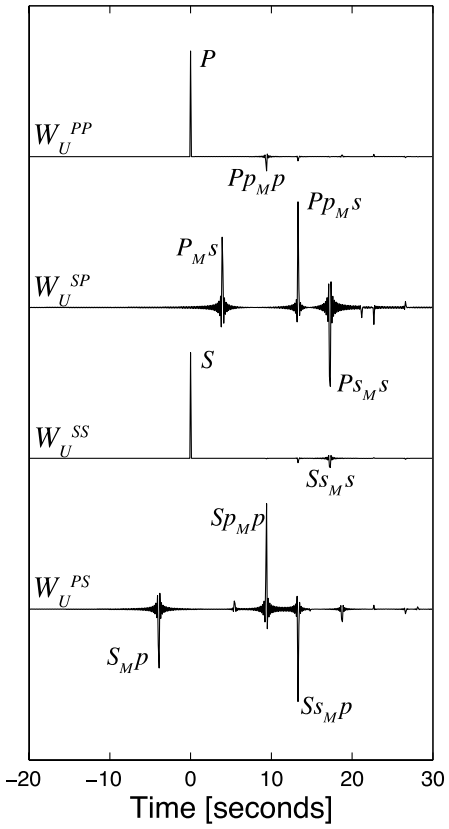

Figure 5. W_U^{PP}, W_U^{SP}, W_U^{SS}, W_U^{PS} components of the Green's functions for a slowness value of 0.05 s/km due to an impulsive source incident below a homogeneous two-layer model mimicking the structure beneath HYB.

however, the effect of inaccuracies in these quantities will be limited through the square root dependence in (8).

[16] Using these quantities we energy normalize the quantities from (7) as

$$W_U^{PP} \Leftarrow \frac{W_U^{PP} C_s^{\alpha}}{C_m^{\alpha}} \qquad W_U^{SP} \Leftarrow \frac{W_U^{SP} C_s^{\beta}}{C_m^{\alpha}},$$
$$W_U^{SS} \Leftarrow \frac{W_U^{SS} C_s^{\beta}}{C_m^{\beta}} \qquad W_U^{PS} \Leftarrow \frac{W_U^{PS} C_s^{\alpha}}{C_m^{\beta}}. \tag{9}$$

4.2.3. Cross Correlation

[17] Upon amplitude balancing and energy normalization, we may perform the cross correlations in (5) to extract energy normalized, free surface reflection seismograms, i.e.,

$$\begin{bmatrix} W^{PP*} & W^{PS*} \\ W^{SP*} & W^{SS*} \end{bmatrix} \begin{bmatrix} W^{PP} & W^{SP} \\ W^{PS} & W^{SS} \end{bmatrix}$$
$$= \begin{bmatrix} W_U^{PP*} W_U^{PP} + W_U^{PS*} W_U^{PS} & W_U^{PP*} W_U^{SP} + W_U^{PS*} W_U^{SS} \\ W_U^{SP*} W_U^{PP} + W_U^{SS*} W_U^{PS} & W_U^{SP*} W_U^{SP} + W_U^{SS*} W_U^{SS} \end{bmatrix}$$
$$= \begin{bmatrix} 1 + V_D^{PP} + V_D^{PP*} & V_D^{SP} + V_D^{PS*} \\ V_D^{PS} + V_D^{SP*} & 1 + V_D^{SS} + V_D^{SS*} \end{bmatrix}, \tag{10}$$

where, recall, V_D is the downward propagating, energy flux normalized wavefield created by the stratification as a result of plane wave incidence from above. Note that the presence of the term 1 within the diagonal elements on the right-hand side of (10) allows one to assign an absolute scale to the response, valid to within the assumptions made in (7) and (9). Only the off-diagonal quantities are changed upon renormalization to displacement, that is

$$V_D^{SP} \Leftarrow \frac{V_D^{SP} C_s^{\alpha}}{C_s^{\beta}} \qquad V_D^{PS} \Leftarrow \frac{U_D^{PS} C_s^{\beta}}{C_s^{\alpha}}. \tag{11}$$

4.2.4. Removal of Free Surface Effect

[18] In the final step, we undo the effect of the free surface reflection to recover the upgoing wavefield for downward incidence, that is,

$$\mathsf{V}_U = \begin{bmatrix} V_U^{PP} & V_U^{PS} \\ V_U^{SP} & V_U^{SS} \end{bmatrix} = \tilde{\mathsf{R}}^{-1} \mathsf{V}_D, \tag{12}$$

where the individual elements of $\tilde{\mathsf{R}}$ are given by, e.g., *Aki and Richards* [2002]. Further note that reciprocity requires $V_U^{SP} = V_U^{PS}$.

5. Examples

5.1. Synthetics

[19] In this section, we demonstrate the applicability of the formalism described above using two sets of synthetic data, one consisting of the full-band impulse response of the medium and the other simulating the band-limited source signatures obtained by convolving the *P* impulse responses with the vertical components of the observed waveforms and those of *SV* with the radial components of the *SKS* waveforms. The impulse responses are generated using the reflectivity method for a single-layer model that mimics the crustal structure beneath Hyderabad [*Saul et al.*, 2000] with the Moho at 32 km depth. Figure 5 shows the W_U^{PP}, W_U^{SP}, W_U^{SS}, W_U^{PS} components of the Green's functions due to an impulsive source, generated for a slowness value of 0.05 s/km. These transmission Green's functions are treated using the procedure outlined in section 4 to obtain the reflection responses shown in Figure 6. We have, however, employed values of surface and mantle velocities within (8) that are significantly underestimated and overestimated, respectively (*P* velocity of 5.5 km/s for the crust and 8.5 km/s for the upper mantle compared to known estimates of 6.55 km/s and 8.1 km/s). For comparison, we plot the true theoretical reflection responses vertically offset with respect to those generated from the transmission seismograms. The two sets of seismograms are visually indistinguishable suggesting that inaccurate a priori estimates of subsurface velocities will lead to errors that are insignificant at the first-order scattering level. In Figure 7 we plot the individual cross correlations $W_U^{PP*} W_U^{SP}$ and $W_U^{PS*} W_U^{SS}$ that contribute to the generation of V_D^{PS} (positive lags) and V_D^{SP*} (negative lags). Because of the minimum phase nature of W_U^{PP} and W_U^{SS}, the cross correlograms are first-order representations of W_U^{SP}, W_U^{PS*} [e.g., *Bostock*, 2004]. It is interesting to note, then, that the forward scattered *P*-to-*S*

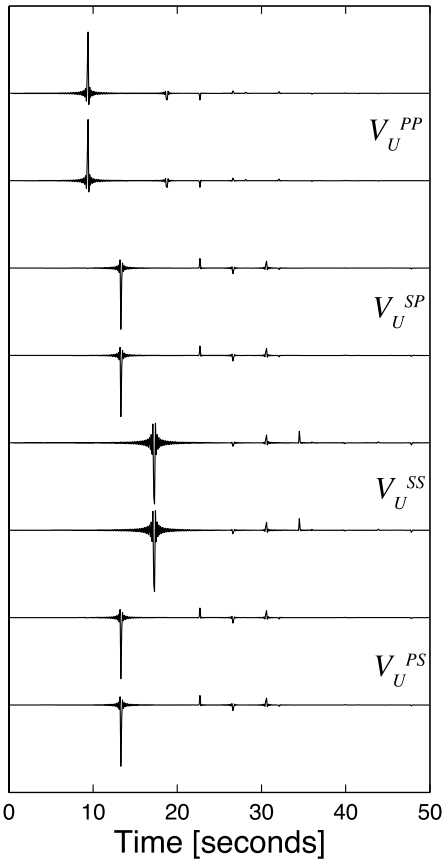

Figure 6. Synthetic *P* and *SV* reflection responses synthesized using the impulse responses in Figure 3. Comparison with the reflection responses obtained employing surface and mantle velocities that are significantly different from the actual ones, plotted with a shift, indicates an exact correspondence.

and *S*-to-*P* arrivals annihilate each other to produce the resulting (back-scattered) reflection seismograms.

[20] To synthesize the band-limited reflection response from source-simulated synthetic transmission seismograms, we employ as sources those observed seismograms representing slowness values in the range of 0.04–0.057 s/km, for both *P* and *SV* (*SKS*) waveforms. The *P* impulse responses convolved with the 300 vertical component seismograms are then used to estimate W^{PP} and W^{SP} Green's functions using the approach outlined in section 2. Similarly, the *SV* impulse responses convolved with the 30 radial component *SKS* waveforms are used to recover the W^{SS} and W^{PS} components of the *SV* Green's functions (Figure 8). The synthesized reflection responses (Figure 9) clearly reveal the direct (V_U^{PP}, V_U^{SS}) and converted (V_U^{SP}, V_U^{PS}) reflected phases. Inaccuracies introduced through source removal may be gauged through the level of disagreement between recovered V_U^{SP} and V_U^{PS}, since these quantities must be, in theory, identical.

5.2. Station HYB (Hyderabad)

[21] Estimates of elements of W_U at station HYB are presented in Figure 3, where, again, the minimum phase nature of W_U^{PP}, W_U^{SS} is apparent. Moreover, distinct first-

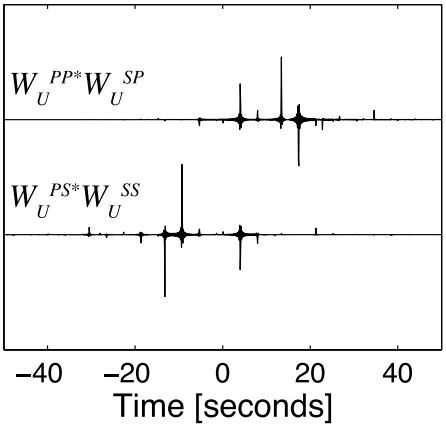

Figure 7. Cross correlations of W_U^{PP}, W_U^{SP} and W_U^{PS}, W_U^{SS} representing the off-diagonal terms in equation (5). Note how the forward scattered *P*-to-*S* and *S*-to-*P* phases annihilate each other to produce the resulting V_D^{PS} and V_D^{SP} reflection responses.

order scattered phases from the Moho are clearly evident on W_U^{PP}, W_U^{SP} and W_U^{PS}, and possibly W_U^{SS}. The *S* Green's function components (W_U^{PS}, W_U^{SS}) are rather noisier due to the relatively small number of high-quality *SKS* seismograms. The synthesized reflection seismograms V_U

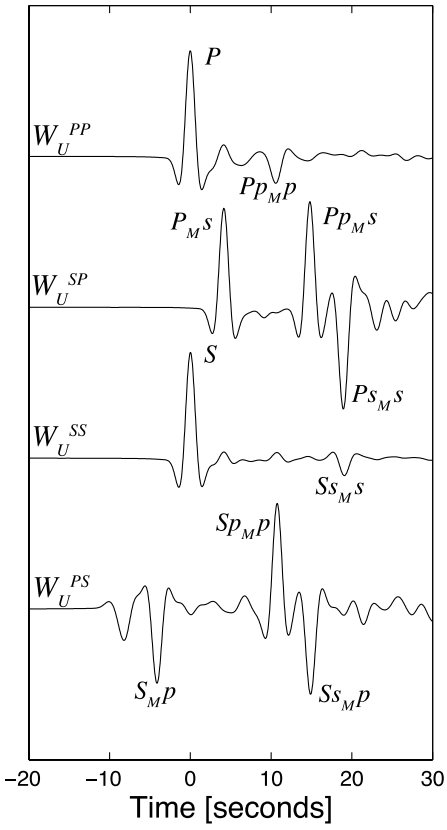

Figure 8. Source simulated *P* and *SV*(*SKS*) Green's functions for HYB in a common slowness range of 0.04–0.0575 s/km band-pass filtered in a range of 0.02–0.5 Hz.

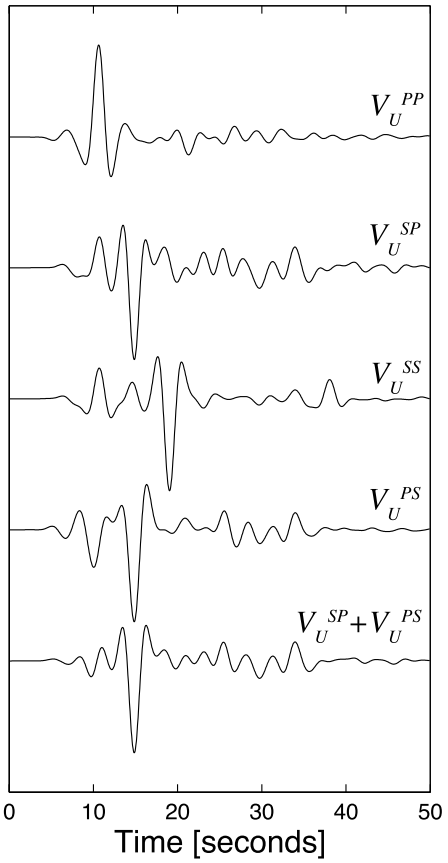

Figure 9. Source simulated *P* and *SV*(*SKS*) reflection responses, band-pass filtered in a range of 0.02–0.5 Hz.

(Figure 10) clearly show the signature of first-order scattering on all but the V_U^{SS} component, and are in general agreement with the synthetic simulation in Figure 9. This component is expected to be the most poorly resolved. Note that the sum $V_U^{SP} + V_U^{PS}$ identifies not only the reflection-conversion from the Moho (near 13 s) but also weaker signals between 20 and 35 s that may correspond to coherent signals evident in Figure 2b between 5 and 10 s likely related to direct *P*-to-*S* conversions from the shallow mantle [*Saul et al.*, 2000].

6. Discussion

[22] In sections 4 and 5 we have shown how readily interpretable reflection seismograms can be generated from observed transmission responses under rather idealized circumstances. These circumstances are, namely, the availability of abundant, high-quality data from a station underlain by dominantly 1-D, isotropic stratification. It is worthwhile considering, therefore, how such results are likely to be impacted by significant departures from ideality and the challenges to be addressed if the methodology is to have practical utility.

[23] Let us first consider the data requirements within the 1-D context for which, in principle, only a single set of *P* and *S* responses at common slowness and frequency is required to accomplish the transmission-to-reflection transformation. Accordingly, the main advantage of an abundant data source is in securing suitable sets of ω, *p* coincident *P* and *S* responses and in reducing the effects of noise through redundancy. In this study we have simplified the former requirement through the assumption of isotropy such that we employ only *P* and *SV* responses. In order to derive reflection seismograms for media with high-contrast, anisotropic layering we would have to measure the anisotropic response due to incident *P* and two incident *S* waves of differing polarization, all sharing a common slowness. In the absence of two independently polarized *S* recordings the resulting reflection seismograms will be incomplete. Note, however, that each cross-correlation term within the matrix on the left-hand side of (5) involves only seismograms corresponding to two components for the same incident mode. Hence for weak contrast stratification, errors in the elements V_U^{PP}, V_U^{PS}, V_U^{SS} (where superscript *S* is meant to denote the single (e.g., *SV*), measured *S* component) of the recovered, reflected wavefield will be correspondingly weak. Note also that the systematic phase shifts produced by shear wave splitting in media with weak but smoothly varying anisotropic (a scenario frequently invoked in the interpretation of *SKS*) are largely undone through the correlations in (5) that take the transmission response into a reflection response.

[24] The most serious source of noise in the analysis of the present study resides in preprocessing removal of

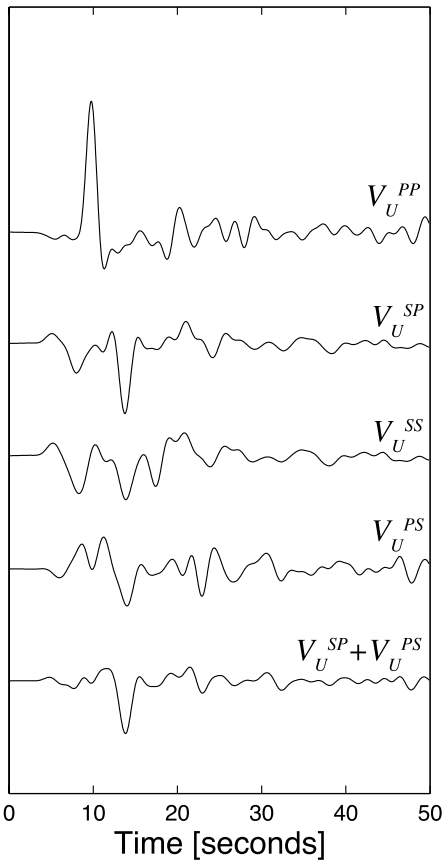

Figure 10. Synthesized *P* and *SV*(*SKS*) reflection responses using the transmission Green's functions, band-pass filtered in the range of 0.02–0.5 Hz. The reflected phases match well with those predicted by the source normalized synthetic responses shown in Figure 9.

earthquake source signatures to produce the required transmission impulse responses or ''Green's functions'', in particular, those components in the incident mode (i.e., scattered P for incident P, scattered S for incident S). The separation of source signature from impulse response is a ''blind deconvolution'' problem. The approach we have used [*Baig et al.*, 2005] is an approximate solution only, even in the absence of noise, although it does benefit from high data redundancy. The clarity of the major Moho-reflected P arrival due to incident teleseismic P within Figure 2a indicates that source removal has been reasonably successful for this contribution. Far fewer data are available, however, for *SKS* which is, moreover, characterized by higher, signal-generated noise levels [see, e.g., *Vinnik and Romanowicz*, 1991]. As a consequence, the estimates of the S to S transmission/reflection impulse responses (i.e., W_U^{SS}/V_U^{SS}) in Figures 8 and 10 are the least reliable. Further improvements in source estimation/removal are the topic of ongoing research and, if successful, should allow 1-D analyses to proceed perhaps even for data from portable experiments since, in principle, only a single set of slowness-coincident recordings is required.

[25] Assuming that more accurate means of source removal become available in the future, we may contemplate the practical extension to laterally heterogeneous media. As mentioned in the introduction, the theory for this task has been developed by *Wapenaar et al.* [2004] such that, for example, the multidimensional analog of equation (5) can be written in the spatial domain as

$$\int_Z \mathrm{d}\mathbf{x}_\perp \, \mathsf{W}_U^*(\mathbf{x}_{\perp A}, \mathbf{x}_\perp, \omega)\mathsf{W}_U^{\mathrm{T}}(\mathbf{x}_{\perp B}, \mathbf{x}_\perp, \omega) = \mathsf{I}\delta(\mathbf{x}_{\perp A} - \mathbf{x}_{\perp B}) + \tilde{\mathsf{R}}\mathsf{V}_U(\mathbf{x}_{\perp A}, \mathbf{x}_{\perp B}, \omega) + \mathsf{V}_U^\dagger(\mathbf{x}_{\perp A}, \mathbf{x}_{\perp B}, \omega)\tilde{\mathsf{R}}^\dagger. \quad (13)$$

Here the integral on the left-hand side is evaluated over the horizontal plane (defined by horizontal coordinate $\mathbf{x}_\perp = (x_1, x_2)$ at a depth $x_3 = Z$ below the (laterally heterogeneous) stratification, $W_U^{\mathrm{T}}(\mathbf{x}_{\perp B}, \mathbf{x}_\perp, \omega)$ is, e.g., the upgoing transmitted wavefield on the surface ($x_3 = 0$) at horizontal coordinate $\mathbf{x}_{\perp B}$ due to a point source at point $\mathbf{x}_\perp$ and depth $x_3 = Z$, $\mathsf{V}_U(\mathbf{x}_{\perp A}, \mathbf{x}_{\perp B}, \omega)$ is the transformed, upgoing reflected wavefield on the surface at horizontal coordinate $\mathbf{x}_{\perp A}$ due to a surface source at $\mathbf{x}_{\perp B}$. Note that sampling requirements have become more stringent because we now require an integral over all possible source points $\mathbf{x}_\perp$ for the upgoing wavefield. Although seemingly intractable for practical purposes, we note that the main contributions to the integral will arise from stationary points [cf. *Wapenaar et al.*, 2005] that may be predictable for weak, lateral heterogeneity, thereby requiring a less complete sampling of the integrand. Moreover, it is likely that successful application for more general circumstances will require that effective interpolation/extrapolation of wavefields [*Abma and Kabir*, 2005] is undertaken as a preprocessing step.

7. Conclusions

[26] For 1-D elastic media comprising stratification bounded by a free surface above and a half-space below, transmission Green's functions at a single (precritical) slowness can be used to recover the corresponding reflection Green's functions. The governing transformation involves cross correlations of the individual transmission components. In principle, this theory requires knowledge of the true relative amplitudes of the P and S components and the material properties underlying the stratification, both of which are generally unknown. We have shown using a combination of synthetic and, importantly, real data (HYB) examples, that reflection responses accurate to first order in scattering can be recovered through a recipe that involves several a priori assumptions. As such we provide a first, albeit idealized, demonstration of the transmission-to-reflection transformation applied to observed, multicomponent seismograms. The importance of this result lies in the potential for isolating different first-order scattering contributions to individual vector components thereby obviating the intereference of forward and back-scattered energy that undermines interpretation of teleseismic transmission (e.g., receiver function) responses, in particular for structures at shallow mantle depths. The feasibility of extending this approach to laterally heterogeneous media will depend upon further improvements in source estimation/removal and the ability to accurately interpolate wavefields.

[27] **Acknowledgments.** We thank Associate Editor Richard Arculus, Hersh Gilbert, and an anonymous reviewer for constructive reviews and Adam Baig and J.-P. Mercier for discussions and help during various stages of this study. R.K. is grateful to the Council of Scientific and Industrial Research, New Delhi, for awarding him the Raman Research Fellowship to pursue research at the University of British Columbia. This research was supported by an NSERC Discovery Grant to M.B.

References

Abma, R., and N. Kabir (2005), Comparisons of interpolation methods, *Leading Edge*, *24*, 984–989.

Aki, K., and P. G. Richards (2002), *Quantitative Seismology*, 2nd ed., 700 pp., Univ. Sci. Books, Herndon, Va.

Baig, A. M., M. G. Bostock, and J.-P. Mercier (2005), Spectral reconstruction of teleseismic P Green's functions, *J. Geophys. Res.*, *110*, B08306, doi:10.1029/2005JB003625.

Bostock, M. G. (2004), Green's functions, source signatures and the normalization of teleseismic wavefields, *J. Geophys. Res.*, *109*, B03405, doi:10.1029/2003JB002783.

Bostock, M. G. (2006), Teleseismic body-wave scattering and receiver-side structure, *Treatise of Solid Earth Geophysics*, vol. 1, edited by B. Romanowicz and A. Dziewonski, Elsevier, New York, in press.

Campillo, M., and A. Paul (2003), Long-range correlations in the diffuse seismic coda, *Science*, *24*, 547–549.

Claerbout, J. F. (1968), Synthesis of a layered medium from its acoustic transmission response, *Geophysics*, *33*, 264–269.

Daneshvar, M. R., C. S. Clay, and M. K. Savage (1995), Passive seismic imaging using microearthquakes, *Geophysics*, *60*, 1178–1186.

Farra, V., and L. P. Vinnik (2000), Upper mantle stratification by P and S receiver functions, *Geophys. J. Int.*, *141*, 699–712.

Frasier, C. W. (1970), Discrete time solution of plane *P-SV* waves in a plane layered medium, *Geophysics*, *35*, 197–219.

Kennett, B. L. N. (1983), *Seismic Wave Propagation in Stratified Media*, 342 pp., Cambridge Univ. Press, New York.

Kennett, B. L. N. (1991), The removal of free surface interactions from three-component seismograms, *Geophys. J. Int.*, *104*, 153–163.

Kumar, P., et al. (2005), The lithosphere-asthenosphere boundary in the north-west Atlantic region, *Earth Planet. Sci. Lett.*, *236*, 249–257.

Mercier, J.-P., M. G. Bostock, and A. Baig (2006), Improved Green's functions for passive source structural studies, *Geophysics*, in press.

Sabra, K. G., P. Gerstoft, P. Roux, W. A. Kuperman, and M. C. Fehler (2005), Surface wave tomography from microseisms in southern California, *Geophys. Res. Lett.*, *32*, L14311, doi:10.1029/2005GL023155.

Saul, J., M. R. Kumar, and D. Sarkar (2000), Lithospheric and upper mantle structure of the Indian shield, from teleseismic receiver functions, *Geophys. Res. Lett.*, *27*, 2357–2360.

Shapiro, N. M., M. Campillo, L. Stehly, and M. H. Ritzwoller (2005), High resolution surface wave tomography from ambient seismic noise, *Science*, *307*, 1615–1618.

Vinnik, L. P. (1977), Detection of waved converted from *P* to *SV* in the mantle, *Phys. Earth Planet. Inter.*, *15*, 39–45.

Vinnik, L., and B. Romanowicz (1991), Origin of precursors to teleseismic *S* waves, *Bull. Seismol. Soc. Am.*, *81*, 1216–1230.

Vinnik, L. P., G. R. Foulger, and Z. Du (2005), Seismic boundaries in the mantle beneath Iceland: A new constraint on temperature, *Geophys. J. Int.*, *160*, 533–538.

Wapenaar, K., J. Thorbecke, and D. Draganov (2004), Relations between reflection and transmission responses of 3-D inhomogeneous media, *Geophys. J. Int.*, *56*, 179–194.

Wapenaar, K., J. Fokkema, and R. Snieder (2005), Retrieving the Green's function by cross-correlation: A comparison of approaches, *J. Acoust. Soc. Am.*, *118*, 2783–2786.

M. G. Bostock, Department of Earth and Ocean Sciences, University of British Columbia, 2219 Main Mall, Vancouver, BC, Canada V6T 1Z4. (bostock@eos.ubc.ca)

M. R. Kumar, National Geophysical Research Institute, Uppal Road, Hyderabad -500 007, India. (kumar_mr1@rediffmail.com)